THE JOURNAL OF BIOLOGICAL CHEMISTRY VOL. 284, NO. 19, pp. 13244–13255, May 8, 2009

Structural Basis for the Antiproliferative Activity of the Tob-hCaf1 Complex*

Received for publication, December 9, 2008, and in revised form, March 9, 2009 Published, JBC Papers in Press, March 10, 2009, DOI 10.1074/jbc.M809250200

Masataka Horiuchi[‡], Kosei Takeuchi[§], Nobuo Noda[‡], Nobuyuki Muroya[‡], Toru Suzuki[¶], Takahisa Nakamura[¶], Junko Kawamura-Tsuzuku[¶], Kiyohiro Takahasi[‡], Tadashi Yamamoto[¶], and Fuyuhiko Inagaki[‡1]

From the [‡]Department of Structural Biology, Graduate School of Pharmaceutical Sciences, Hokkaido University, N12, W6, Kita-ku, Sapporo 060-0812, Japan, the [§]Division of Molecular and Cellular Biology, Graduate School of Medical and Dental Sciences, Niigata University, Asahi-machi, Chuo-ku, Niigata 951-8510, Japan, and the [¶]Department of Oncology, Institute of Medical Science, University of Tokyo, 4-6-1 Shiroganedai, Minato-ku, Tokyo 108-8639, Japan

The Tob/BTG family is a group of antiproliferative proteins containing two highly homologous regions, Box A and Box B. These proteins all associate with CCR4-associated factor 1 (Caf1), which belongs to the ribonuclease D (RNase D) family of deadenylases and is a component of the CCR4-Not deadenylase complex. Here we determined the crystal structure of the complex of the N-terminal region of Tob and human Caf1 (hCaf1). Tob exhibited a novel fold, whereas hCaf1 most closely resembled the catalytic domain of yeast Pop2 and human poly(A)-specific ribonuclease. Interestingly, the association of hCaf1 was mediated by both Box A and Box B of Tob. Cell growth assays using both wild-type and mutant proteins revealed that deadenylase activity of Caf1 is not critical but complex formation is crucial to cell growth inhibition. Caf1 tethers Tob to the CCR4-Not deadenylase complex, and thereby Tob gathers several factors at its C-terminal region, such as poly(A)-binding proteins, to exert antiproliferative activity.

The Tob/BTG family (also called the APRO family) is a group of antiproliferative proteins (1, 2) consisting of Tob (3), Tob2 (4), BTG1 (5), BTG2/Tis21/PC3 (6–8), PC3B (9), and ANA/BTG3 (10, 11) in mammalian cells, AF177464 in *Drosophila*, and FOG-3 in *Caenorhabditis elegans* (12). A recent genome project reported that the BTG/Tob family protein had already existed in Choanoflagellida *Monosiga brevicollis* MX1. The N-terminal region of the Tob/BTG family proteins is conserved and includes two highly homologous regions, Box A and Box B. The Tob/BTG family proteins are involved in cell cycle regulation in a variety of cells such as T lymphocytes, fibroblasts, epithelial cells, and germ cells. In Tob-deficient mice, the incidence of liver tumors is higher than in wild-type mice. Furthermore, because the levels of *tob* expression are often repressed in human lung cancers, suppression of its expression is thought to contribute to tumor progression (13).

The antiproliferative activities of the Tob/BTG family proteins are due to their association with target proteins in cells. For example, Tob associates with SMAD family proteins and acts as a negative regulator of SMAD signaling. In osteoblasts, this negative regulation occurs via association with SMAD 1, 5, 6, and 8 (14, 15), and via association with SMAD 2 and 4 in anergic quiescent T cells (16). Tob/BTG family proteins also bind to protein arginine methyltransferase, which regulates chromatin assembly by histone methylation (17). Much evidence has been accumulated to suggest that CCR4-associated factor 1 (Caf1),[2] also known as Cnot7 and involved in the CCR4-Not deadenylase complex, is a common binding partner of the Tob/BTG family proteins (4, 18–21). To reveal the functions of Caf1 *in vivo*, *caf1*$^{-/-}$ mice have been generated in two groups. Male *caf1*-deficient mice are infertile because of a malfunction of the testicular somatic cells that leads to a defect in spermatogenesis (22, 23). Genetic analysis of the nematode *C. elegans* also suggests that FOG3 (Tob orthologue) interacts with CCF1, the *C. elegans* homologue of Caf1, and that this interaction is essential for germ cells to initiate spermatogenesis (24).

Mouse and human Caf1 (mCaf1 and hCaf1) were found as homologues of yeast Pop2, a component of the CCR4-Not complex (18, 25). Yeast Pop2 displays weak RNase activity but enhances the deadenylation of the poly(A) tail of mRNA by the CCR4-Not deadenylase complex (26–29). The primary structure of mammalian Caf1 is related to that of the ribonuclease D (RNase D) family, and all of the active site residues are well conserved (30). Indeed, both mCaf1 and hCaf1 have deadenylase activity (31–33).

Although the relationship between cell cycle repression and poly(A) deadenylation is not well understood, mRNA degradation and synthesis are major events in maintaining the cell cycle (34). The mRNAs in a eukaryotic cell have a wide range of half-lives. Degradation of mRNA is initiated by shortening of the poly(A) tail. Thereafter, the 5′-cap structure is removed and

* This work was supported by Grant-in-aid for Scientific Research 15770063 and the National Projects on Protein Structural and Functional Analyses and Targeted Proteins Program from the Ministry of Education, Culture, Sports, Science, and Technology, Japan.

[1] To whom correspondence should be addressed. Tel.: 81-11-706-9011; Fax: 81-11-706-9012; E-mail: finagaki@pharm.hokudai.ac.jp.

[2] The abbreviations used are: Caf1, CCR4-associated factor 1; m, mouse; h, human; PABP, poly(A)-binding protein; PABPC1, cytoplasmic poly(A)-binding protein; CNS, crystallography and NMR system; MIR, multiple isomorphous replacement; PARN, poly(A)-specific ribonuclease; FITC, fluorescein isothiocyanate; DTT, dithiothreitol; GST, glutathione *S*-transferase; HEK, human embryonic kidney; HRP, horseradish peroxidase; PDB, Protein Data Bank; PARN, poly(A)-specific ribonuclease; ERK, extracellular signal-regulated kinase; NES, nuclear export signal; YFP, yellow fluorescent protein; CFP, cyan fluorescent protein.

the remaining portion of the mRNA is rapidly degraded. The degradation of eukaryotic mRNAs is regulated precisely at each stage of the cell cycle. Tob was reported to associate with inducible poly(A)-binding protein (iPABP) and to abrogate the translation of interleukin-2 mRNA *in vitro* (35). Recent reports also showed that Tob and BTG2 interact with the CCR4-Not deadenylase complex using the Tob/BTG2 domain and the cytoplasmic poly(A)-binding protein (PABPC1) using the C-terminal tail and enhanced mRNA degradation (36–38).

To help elucidate the relationship between the antiproliferative activity of Tob and the degradation of the poly(A) tail, we determined the crystal structure of the Tob-hCaf1 complex. We found that hCaf1 has a structure similar to yeast Pop2 and human PARN of deadenylases, exonuclease I, and the Klenow fragment of DNA polymerase I from *Escherichia coli*. In contrast, Tob has a novel structure. Specifically, Box A and Box B mediate the interaction between Tob and hCaf1. Cell growth assays using the wild and mutant proteins, together with the structural studies, revealed that the complex formation is crucial to cell growth inhibition.

EXPERIMENTAL PROCEDURES

Bacterial Expression, Purification, and Crystallization of the TobN138-hCaf1 Complex—The antiproliferative region of human Tob comprising the N-terminal 138 residues (which is termed TobN138) and intact hCaf1 were co-expressed in *E. coli*. The gene of TobN138 was subcloned under a hexahistidine tag (His_6) into the pHT1 plasmid derived from the pET-28 plasmid (Novagen), and the gene of hCaf1 was subcloned into the pET-11 plasmid (Novagen). These plasmids were co-transformed in *E. coli* BLR(DE3) pLysS for native proteins and methionine-auxotroph strain B834(DE3) for SeMet-labeled proteins. Cells were cultured to an A_{600} of 0.5 at 30 °C and induced with 1 mM isopropyl-β-D-thiogalactopyranoside for 18 h. After cell lysis, the protein was applied to nickel-nitrilotriacetic acid-agarose resin (Qiagen) and eluted with a gradient of 0–250 mM imidazole in 50 mM Tris-HCl (pH 8.0), 150 mM NaCl, and 1 mM 4-(2-aminoethyl)-benzenesulfonyl fluoride. The HisTobN138-Caf1 complex was separated from the HisTobN138 monomer using a Superdex 75pg 26/60 gel filtration column (GE Healthcare) equilibrated with 50 mM Tris-HCl (pH 8.0), 150 mM NaCl, and 0.5 mM EDTA. The heterodimer fraction was loaded onto a MonoQ HR10/10 anion exchange column (GE Healthcare) equilibrated with 20 mM Tris-HCl (pH 8.0). The heterodimer was eluted using a 160-ml linear gradient of 0 to 1 M NaCl. Fractions containing the heterodimer were dialyzed against 10 mM Tris-HCl (pH 8.0), 30 mM NaCl, 0.1 mM EDTA, and 5 mM dithiothreitol (DTT) and then stored at −80 °C prior to crystallization. The purified protein complex was concentrated to 20 mg/ml and used for crystallization.

In the sitting drop vapor diffusion method, 1 μl of 20 mg/ml HisTobN138-hCaf1 complex (10 mM Tris-HCl (pH 8.0), 30 mM NaCl, 0.1 mM EDTA, and 5 mM DTT) was mixed with an equal volume of a reservoir solution (80 mM Tris-HCl, pH 8.0, 160 mM sodium acetate, 10 mM DTT, 12% (w/v) polyethylene glycol 4000, and 12% glycerol). The protein-reservoir mixture was incubated with 100 μl of reservoir at 20 °C and small crystals (<0.02 mm) were obtained after 24 h. To prepare the seed-stock, 1 μl of drop containing small crystals was diluted with 30 μl of the same reservoir solution and vortexed with a Teflon ball (Hampton) in a micro tube. 1 μl of the serial dilutions (10^{-1}-10^{-8}-fold) of seed stock was mixed with 1 μl of 20 mg/ml protein solution and incubated at 20 °C with 100 μl of reservoir. After 48 h at 20 °C, microseeding generated crystals of 0.3 × 0.3 × 0.1 mm. To prepare heavy atom derivatives, crystals were soaked at 20 °C in reservoir solutions without DTT and EDTA and containing either 1 mM neodymium chloride (for 20 h) or 0.1 mM methyl mercuric acetate (for 1 h).

The crystal of the active form was prepared by soaking the crystal for 12 h at 20 °C in a reservoir solution without DTT or EDTA but with 1 mM $MnCl_2$. Prior to data collection, crystals were cryoprotected by incubation for 5 min in a reservoir solution containing 15% polyethylene glycol 4000 and 30% glycerol. After soaking, the crystals were mounted on cryoloops (Hampton) and frozen in liquid nitrogen.

Data Collection, Structural Analysis, and Refinement—All data for the hCaf1-HisTobN138 complex were collected using synchrotron radiation with a PX210 CCD detector (Oxford) at the Osaka University Beam Line BL44XU in Spring-8 at −173 °C. Diffraction data were processed using the MOSFLM program, and intensities were scaled using SCALA in the CCP4 program suite and HKL2000 programs. The structure was phased by multiple isomorphous replacement (MIR) using the crystallography and NMR system (CNS) program. The heavy atom positions of the neodymium derivative were found by inspection of the Patterson map, and those of other derivatives were identified by Fourier difference methods. The initial MIR phase had a mean figure of merit of 0.50 at a resolution of 4.0 Å and was improved by density modification using the CNS program. A model was built into the MIR electron density maps using the TURBO-FRODO program. After rigid-body refinement and simulated annealing with CNS, several rounds of model building with TURBO-FRODO and refinement with CNS were carried out, with the refinement converging to a final *R*-factor of 22.3% (R_{free} = 24.6%) for all data at a resolution of 2.5 Å. The crystal structure of the complex with manganese ions was determined by using the model of the structure without metal ions. By further refinement, a final *R*-factor of 22.7% (R_{free} = 25.9%) for all data at a resolution of 2.7 Å was obtained. The diffraction data and refinement statistics are shown in Table 1.

In Vitro Nuclease Assays—The following commercially synthesized 5′-fluorescent dye-labeled RNA substrates were used: RNA-A6 (5′-fluorescein isothiocyanate (FITC)-GAC UGA CUA AAA AA-3′), RNA-C6 (5′-FITC-GAC UGA CUC CCC CC-3′), RNA-U6 (5′-FITC-GAC UGA CUU UUU UU-3′), RNA-A7 (5′-FITC-UGA UAG UAC AAAAAAA-3′) (Fasmac). The enzymatic reaction mixture (50 μl) consisted of 1 μM 5′-FITC RNA substrate, GST-hCaf1 (0.5 or 2 μM) in the presence or absence of HisTobN138 (0.25, 0.5, 1, 2 μM), 20 mM HEPES-NaOH (pH 7.4), 150 mM NaCl, 10 mM metal ions ($MgCl_2$, $CaCl_2$, $MnCl_2$, or $CoCl_2$), and 1 mM DTT were incubated at 37 °C. The reaction was stopped by the addition of an equal volume of formamide. 10 μl of the reaction mixtures were loaded onto an 8 M urea-20% polyacrylamide denaturing sequencing gel and separated by electrophoresis. The 5′-FITC

RNA substrate bands were detected and quantified using either an FLA-2000 fluorescence imager or LAS-4000mini and accompanying software (Fujifilm).

In Vitro Binding Assay—The genes for wild-type hCaf1 (*hcaf1-wild*) and the Lys-203c to Ala mutant of the interaction surface of hCaf1 (*hcaf1-k203a*) were cloned into pGEX-6P vector (GE Healthcare) for expression of GST-fused proteins. GST-hCaf1-wild and GST-hCaf1-K203A were expressed in *E. coli* DH5α and purified by glutathione-Sepharose 4B resin (GE Healthcare) according to the manufacturer's protocols. For binding assays, 500 μl of either GST-hCaf1-wild or GST-hCaf1-K203A was loaded with HisTobN138 (final concentration 3.5 μM of each protein) on the gel-filtration column of Superdex 200 10/300GL (GE Healthcare) equilibrated with 20 mM Tris-HCl (pH 8.0), 150 mM NaCl at 1 ml/min at 25 °C. The elution fractions were analyzed by SDS-PAGE.

Construction of Plasmids for Affinity Precipitation and Growth Assay—The genes for *tob* and *hcaf1* were constructed by fusing *tob* to *flag* and *hcaf1* to *strep-tag II*, respectively, by an overlap extension PCR technique. The genes for *eyfp-tob* and *ecfp-hcaf1* were also constructed by fusing *eyfp*, which was amplified from pEYFP plasmid (Clontech), to *tob* and *ecfp*, which was amplified from pEYFP plasmid (Clontech), to *hcaf1*, respectively. The obtained DNA fragments were cloned into the pENTR/SD/D-TOPO plasmid by TOPO reaction and were further transferred to the pLenti4/TO/V5-DEST expression plasmid by LR reaction (Invitrogen). The site-directed mutagenesis for the construction of *tobn138*, *hcaf1-d40n*, *hcaf1-k203a*, *eyfp-tobn138*, *ecfp-hcaf1-d40n*, and *ecfp-hcaf1-k203a* genes were performed by using an overlap extension PCR technique. These genes were also cloned into the pENTR/SD/D-TOPO plasmid and were further transferred to the pLenti4/TO/V5-DEST expression plasmid.

Cell Culture—HEK-293, 293FT cells (human embryonic kidney cells), COS-1 cells, and NIH3T3 cells were maintained in growth medium (high glucose Dulbecco's modified Eagle's medium (Invitrogen) supplemented with 10% heat-inactivated fetal bovine serum (HyClone, Melbourne, Australia)). Cells were grown at 37 °C in a humidified atmosphere of 5% CO_2.

Affinity Precipitation Assay—The expression plasmids were transfected into 293FT cells. After 48 h, cells were washed with phosphate-buffered saline and then lysed with CelLytic™ M (Sigma-Aldrich) containing a protease inhibitor mixture (Nakarai). The lysates were clarified by centrifugation and incubated with either anti-FLAG M2 affinity gel (Sigma-Aldrich) or Strep-Tactin-Sepharose fast flow gel (IBA). The gels were then washed with TBS (25 mM Tris-HCl (pH 7.5), 150 mM NaCl), and the precipitates were eluted by 3× FLAG peptide in TBS from the anti-FLAG M2 affinity gel or 2.5 mM *d*-desthiobiotin in 100 mM Tris-HCl (pH 8.0), 150 mM NaCl, 1 mM EDTA from the Strep-Tactin-Sepharose fast flow gel. The eluted proteins were resolved by SDS-PAGE and electroblotted onto polyvinylidene difluoride filters. After blocking by 3% bovine serum albumin or 5% skim milk, the filters were incubated with HRP-conjugated anti-FLAG M2 (Sigma-Aldrich) or HRP-conjugated anti-Strep-tag II antibodies (IBA) and treated with HRP substrate for detection by chemical luminescence (Millipore).

Stable and Transient Transfection of Cells and Cell Growth Analysis—DNA fragments encoding FLAG-tagged Tob and FLAG-tagged hCaf1 proteins were cloned into the pMX-puro vector for retroviral production (39, 40). NIH3T3 cells were infected with recombinant retrovirus and cultured in the presence of puromycin, and 1×10^3 cells were seeded in 60-mm dishes. Ten days after seeding, colonies were stained by using the Giemsa staining method. For the transfection analysis, we used the Nucleofector kit for cell lines (Amaxa Biosystems) according to the manufacturer's protocol for transfection. Cells were trypsinized (attached cell lines) and resuspended in Nucleofector solution at a final concentration of 1×10^6 cells/100 μl. We then mixed 100 μl of cell suspension with 2–8 μg of plasmid DNA and transferred the nucleofection sample into a 0.2-cm certified cuvette (2.0 mm in width). The suspension was electroporated with an Amaxa Nucleofector apparatus using an appropriate program for each cell line. Immediately after electroporation, the transfected cells were resuspended in prewarmed medium. The transfected cells were plated in 35-mm culture dishes. At 18 h after transfection, cells were then pelleted by centrifugation and resuspended at the appropriate cell concentrations in phosphate-buffered saline. Flow cytometric analysis was performed using a FACS Vantage SE flow cytometer (BD Biosciences). The induced gene-expressed cells were collected on the basis of their enhanced yellow fluorescent protein (EYFP; Tob expression) and enhanced cyan fluorescent protein (ECFP; Caf1 expression) intensity. The dead cells and non-expressing cells were eliminated based on their intensity with EYFP, ECFP, and the vital dye propidium iodide (from Dojindo). To determine the effect of regulation by Tob or Caf-1 on cell proliferation, cells were seeded at 5×10^4 cells/well and incubated for 90 h. To determine the rate of cell growth, cells were harvested by trypsinization and counted manually in triplicate using a hemocytometer and a flow cytometer for accuracy. Determination of the expression level of the proteins was performed by electrophoresis or immunostaining in glass coverslips following the above cell assays. For the selection of stably transfected cells, neomycin selection was applied with the addition of 300 μg/ml (COS-1) or 400 μg/ml (HEK-293, NIH3T3) G418 (Invitrogen) at 24 h after transfection and maintained for 2 weeks. Neomycin-resistant colonies were picked manually and cultured in the presence of G418. As described under "Results" and "Discussion," the expressions of many wild-type or mutated forms of Tob/Caf1 also resulted in the expression of almost equal levels of proteins during the cell growth analysis.

RESULTS

Structure of the Tob-hCaf1 Complex—To elucidate how Tob recognizes hCaf1 in the growth repression complex, we determined the crystal structure of the Tob-hCaf1 complex. First, we tried to produce recombinant intact Tob in *E. coli*. However, it was difficult to purify intact Tob because of degradation. As both Box A and Box B of BTG/Tob family proteins are sufficient to associate with hCaf1, we next coexpressed an antiproliferative region of human Tob comprising the N-terminal 138 residues (which we refer to as TobN138) and intact hCaf1 in *E. coli* BLR(DE3). The crystal of the TobN138-hCaf1 complex in the absence of metal ions contained one heterodimer molecule in

TABLE 1

Data collection and refinement statistics

Highest resolution shells are shown in parentheses. r.m.s., root mean square.

	Native	$NdCl_3$	$CH_3COOHgCH_3$	SeMet	$MnCl_2$
Data collection					
Space group	*I*422	*I*422	*I*422	*I*422	*I*422
Cell dimensions					
a, *b*, *c* (Å)	151.5, 151.5, 114.2	151.9, 151.9, 114.1	152.2, 152.2, 114.7	151.7, 151.7, 114.3	150.9, 150.9, 113.9
α, β, γ (°)	90, 90, 90	90, 90, 90	90, 90, 90	90, 90, 90	90, 90, 90
Resolution (Å)	58-2.5 (2.6-2.5)	76-3.1 (3.3-3.1)	48-4.0 (4.2-4.0)	58-2.7 (2.9-2.7)	58-2.7 (2.9-2.7)
R_{merge}	10.3 (26.8)	13.2 (27.0)	9.5 (12.8)	13.8 (23.5)	10.6 (26.5)
I/sI	3.8 (1.8)	4.3 (2.3)	6.7 (5.0)	3.5 (2.1)	4.6 (30.5)
Completeness (%)	97.9 (98.9)	94.9 (94.9)	99.9 (99.9)	99.9 (99.9)	100 (100)
Refinement					
Resolution (Å)	2.5				2.7
No. reflections	23,275				17,925
R_{work}/R_{free}	22.3/24.6				22.7/25.9
No. atoms					
Protein	3,023				3,005
Ligand/ion	0				Mn^{2+} 2
Water	90				0
B-factors					
Protein	47.1				56.7
Ligand/ion	0				Mn^{2+} 53.3
Water	49.3				
r.m.s. deviations					
Bond lengths (Å)	0.007				0.008
Bond angles (°)	1.26				1.21

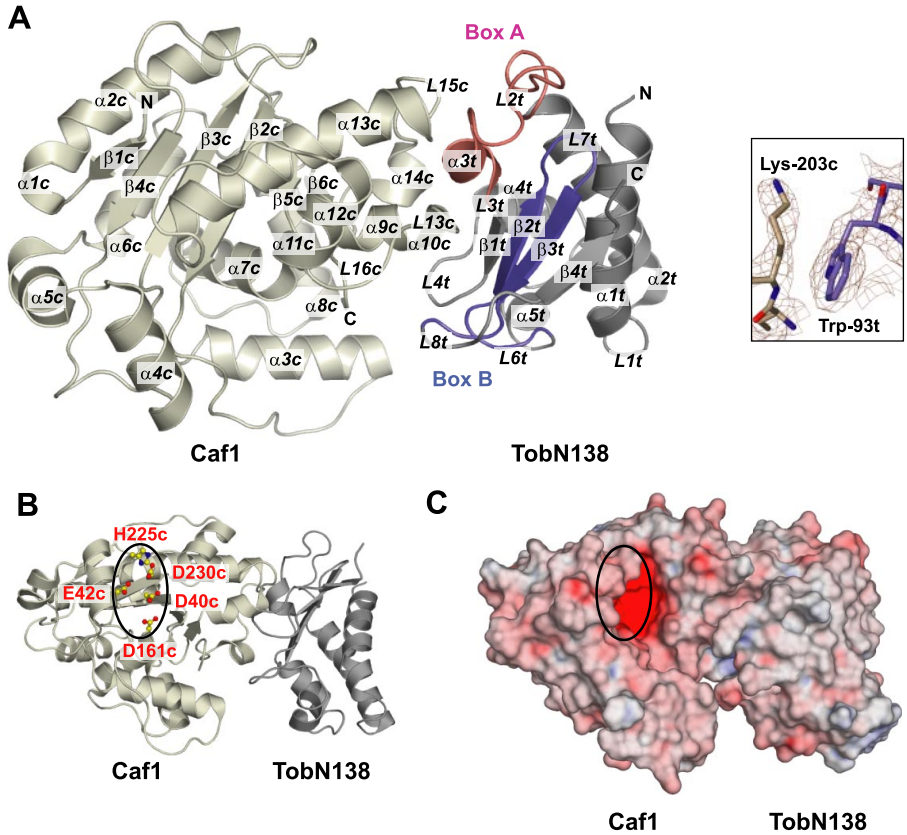

FIGURE 1. **Structure of the TobN138-hCaf1 complex.** *A*, ribbon diagram of the TobN138-hCaf1 complex labeled with secondary structures. hCaf1 is shown in *light yellow* and TobN138 in *gray*. Box A and Box B of Tob are shown in *red* and *blue*, respectively. The $F_o - F_c$ omit map of the interacting residues of Trp-93t and Lys-203t at 1.0 σ contour level is displayed in the *right panel*. *B*, the side chains of the active site residues, enclosed by a *circle*, are shown as *ball-and-stick* models. *C*, the electrostatic surface potential of the hCaf1-TobN138 complex calculated by GROMACS. The view shown is from the same orientation as in *B*. Figs. 1, 4, and 5 were prepared with PyMOL.

an asymmetric unit. We determined the crystal structure of TobN138-hCaf1 at 2.5 Å resolution by MIR. The current refinement model has an *R*-factor of 22.3% and an R_{free} of 24.6% (Table 1; PDB entry 2d5r).

We constructed an atomic model for the TobN138 region from residue 1 to 115 and for the hCaf1 region from residue 11 to 262 (Fig. 1*A*), other regions were disordered in the electron density map. We found that TobN138 is folded into an α/β structure with an antiparallel β-sheet consisting of four β-strands supported by a helix bundle containing two long helices and three short helices. Further, hCaf1 is folded into an α/β structure with an open, twisted mixed β-sheet of six β-strands surrounded by 14 α-helices.

The largest association surface between TobN138 and hCaf1 is composed of helix α3t, strands β1t, β2t, and β3t, and loops L2t, L3t, L4t, L7t, and L8t of TobN138 along with helices α10c and α14c and loops L13c, L15c, and L16c of hCaf1 (Fig. 1*A*). The buried surface area between TobN138 and hCaf1 is 1511 $Å^2$. Interestingly, Box A (Fig. 1*A*, in *red*) and Box B (in *blue*) of Tob mediate the association with hCaf1. The β-sheets containing β1t, β2t, and β3t are supported by two long α-helices (α1t and α2t). These helices contain hydrophobic residues that are well conserved in the Tob/BTG family (Ile-5t, Phe-28t, Leu-32t, and Leu-36t) and are located at the hydrophobic interface with the β-sheet that presents Box B to hCaf1. The electrostatic surface potential of TobN138-hCaf1 complex

reveals the presence of an acidic pocket, which was identified as the active site (Fig. 1, *B* and *C*).

Structure-based Sequence Alignment of TobN138 and hCaf1 by DALI Search—To help predict some of the physiological functions of the TobN138-hCaf1 complex, we applied the coordinate data of hCaf1 and TobN138 to the DALI server. We found that hCaf1 is structurally similar to some nucleases including Pop2 of *Schizosaccharomyces pombe* and *Saccharomyces cerevisiae* (Z-scores of 39.5 and 30.0 for PDB entries 2p51 (41) and 1uoc (42)), respectively, Poly(A)-specific ribonuclease PARN of *Homo sapiens* (Z-score of 23.1 for PDB entry 2a1r (43)), the N-terminal exonuclease domain of the ϵ-subunit of *E. coli* DNA polymerase III (Z-score of 14.8 for PDB entry 1j53 (44)), exonuclease I of *E. coli* (Z-score of 13.5 for PDB entry 1fxx (45)), and the Klenow fragment-like DNA polymerase of *Bacillus stearothermophilus* (Z-score of 9.4 for PDB entry 1xwl (46)).

On the other hand, only two structures similar to TobN138 were identified by DALI search: the structures of the BTG/Tob domain of Tob (Z-score of 24.0 for PDB entry 2z15) and that of BTG2 (Z-score of 20.4 for PDB entry 3e9v). Therefore, it appears that TobN138 is a typical structural domain for the BTG/Tob family. On the basis of the results of the DALI search, we made structure-based sequence alignments for Tob and Tob/BTG family proteins (Fig. 2*A*) and for hCaf1 and RNase D family proteins (Fig. 2*B*).

Requirement of Metal Ions for hCaf1 Nuclease Activity—The structure of hCaf1 is composed of the core catalytic domain of the RNase D superfamily, which is characterized by the DEDD sequence motif. These conserved acidic amino acids are responsible for metal ion binding involved in catalysis. Although the crystal structure of hCaf1 was solved in the absence of metal ions, we identified two neodymium ions in the active site of the acidic surface in a derivative used for MIR analysis. For this reason, we examined the nuclease activity of hCaf1 in the presence of Mg^{2+}, Ca^{2+}, Mn^{2+}, and Co^{2+}. First, hCaf1 and 14-mers of 5′-FITC-labeled single-stranded DNA and RNA were mixed with each of the metal ions and incubated at 37 °C (Fig. 3*A*). Short DNA or RNA fragments were observed in the presence of Mg^{2+}, Mn^{2+}, and Co^{2+} but not Ca^{2+}, and hCaf1 showed much higher catalytic activity with RNA than with DNA as the substrate. RNase activity in the presence of Mn^{2+} was higher than in the presence of Mg^{2+} or Co^{2+}. Thus, Mn^{2+} is required for hCaf1 to exhibit full RNase activity. It should be also noted that after digestion, 5′-terminal trinucleotides of the RNA substrate remained, suggesting that at least three nucleotides are required for binding to the active site of hCaf1.

Previous reports have indicated that mammalian Caf1 has poly(A)-specific deadenylase activity (31, 33, 36). To determine whether hCaf1 used in the crystallization studies has poly(A)-specific deadenylase activity, we performed nuclease assays in the presence of Mn^{2+} using single-stranded RNA substrates including hexaadenine (A6), hexacytosine (C6), and hexauracil (U6) attached to the 3′-end of a 5′-FITC-labeled 8-mer RNA. We found that 3′-digestion of A6 by hCaf1 was much faster than 3′-digestion of C6 and U6 (Fig. 3, *B* and *C*). The ability of hCaf1 to cleave hexaguanine was not studied because it was difficult to synthesize. Because hCaf1 prefers a poly(A) tail to a poly(C) or a poly(U) tail on single-stranded RNA as a substrate, we concluded that hCaf1 is an exonuclease with poly(A) deadenylase activity in the presence of Mn^{2+}.

To examine whether deadenylation activity of hCaf1 is affected by BTG/Tob domain *in vitro*, nuclease assays of GST-hCaf1 in the presence of HisTobN138 were performed. There was no appreciable effect on the activity of hCaf1 in the presence of TobN138, although 4 molar excess of TobN138 was added (Fig. 3*D*, *left panel*).

Comparison of the Structure of the Active Sites of hCaf1 and hPARN—Because Mn^{2+} is required for the catalytic activity of hCaf1, we soaked the crystal of Tob-hCaf1 with a solution containing $MnCl_2$. The crystal structure was determined at 2.7 Å resolution with an *R*-factor of 22.7% and R_{free} of 25.9% (Table 1). The active site structure of the Tob-hCaf1 complex is shown in Fig. 4*A* together with that of hPARN deadenylase bound to the single-stranded RNA substrate (PDB entry 2a1r (43)). The Tob-hCaf1 complex binds two manganese ions (Mn-A and Mn-B; Fig. 4*A*, *red spheres*) at positions similar to the two metal ion-binding sites of the exonuclease domain of hPARN. The carboxylate groups of Asp-40c, Asp-230c, and Glu-42c associate with Mn-A, whereas those of Asp-40c and Asp-161c associate with Mn-B.

Some of the active site residues of RNase D family nucleases have been predicted based on the primary sequences. Asp-40c, Glu-42c, Asp-161c, Asp-230c, and His-225c of hCaf1 can be aligned with the active site residues of the RNase D family proteins (Fig. 2*B*). These acidic residues of hCaf1 bind to manganese ions, and His-225c serves as the general base in the two-metal ion mechanism. To determine whether the five conserved residues of hCaf1 act as catalytic residues, we performed a site-directed mutation study. Asp-40c, Glu-42c, Asp-161c, His-225c, and Asp-230c of hCaf1 were individually changed to Asn-40c, Gln-42c, Asn-161c, Ala-225c, and Asn-230c. Incubation of these mutants with A6-RNA in the presence of Mn^{2+} did not result in cleavage (Fig. 4*B*). Thus, these five conserved residues are critical catalytic residues of hCaf1. In yeast Pop2, the residues corresponding to Asp-40c, His-225c, and Asp-230c of hCaf1 are replaced by Ser, Thr, and Gln, respectively, resulting in much lower deadenylase activity compared with hCaf1.

The phosphate backbone at the 5′-site is recognized by Asn-288p in hPARN, which correspond to His-157c in hCaf1. The hydrophobic side chain of Ile-34p in hPARN, which corresponds to Val-46c in hCaf1, is flanked by the 3′-end and the penultimate bases. Moreover, the 3′-end base is stacked with Phe-115p of hPARN. In hCaf1, this position is occupied by Leu-115c (Fig. 4*A*). Taken together, these results suggest that the base recognition and the catalytic mechanism of hCaf1 are similar to those of hPARN.

Interaction Surface between Tob and hCaf1—The major interaction surface between TobN138 and hCaf1 contains regions composed of both Box A and Box B (Figs. 1*A* and 5*A*), indicating that the conserved regions in Tob/BTG family proteins are crucial for their binding. Conserved residues Trp-93t, Asp-95t, and Glu-98t in Box B play pivotal roles in the interaction with hCaf1; Asp-95t and Glu-98t form salt bridges with Lys-203c, and Trp-93t inserts its side chain into the hydropho-

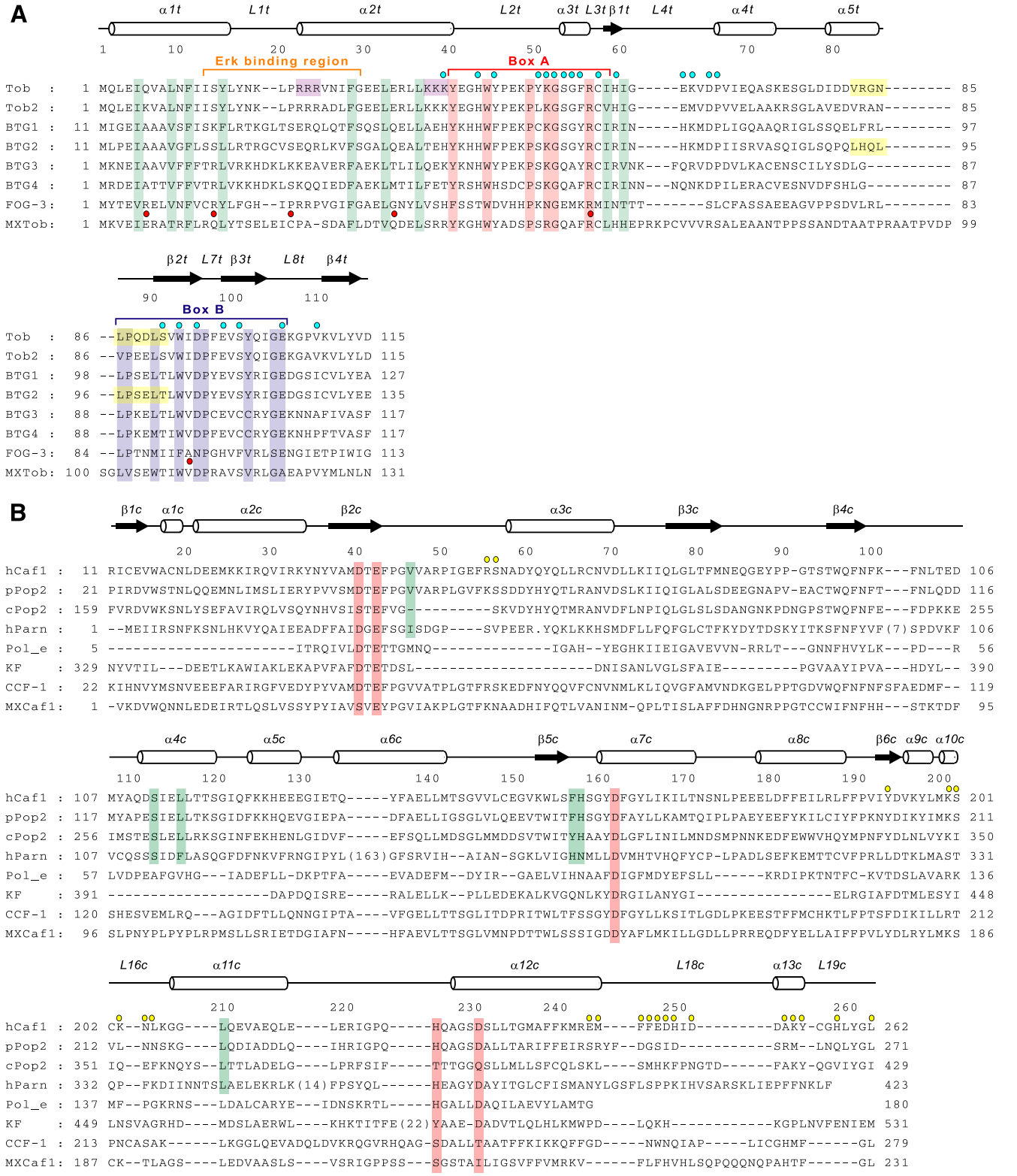

FIGURE 2. **Sequence alignments of Tob and hCaf1 with related proteins.** *A*, sequence alignment of human Tob, Tob2, BTG1, BTG2, BTG3, FOG-3, and Tob-like protein of *M. brevicollis* MX1 (MXTob). The conserved residues in the Box A and Box B regions of BTG family proteins are shown in *red* and *blue*, respectively. The *blue dots* on the sequence denote the buried residues involved in the interaction surface with hCaf1. The *red dots* below the sequence denote the missense mutation sites in FOG-3. The conserved residues required for the maintenance of the hydrophobic core of the BTG domain are colored *green*. The basic residues for nuclear localization are shown in *purple*. The residues for nuclear export are shown in *yellow*. The region required for ERK binding is indicated by an *orange line*. The secondary structure of TobN138 is shown *above* of the sequences. *B*, sequence alignment of human Caf1 (hCaf1), *S. pombe* Pop2 (pPop2), *S. cerevisiae* Pop2 (yPop2), human poly(A)-specific ribonuclease PARN (hParn), the N-terminal exonuclease domain of the ϵ subunit of *E. coli* DNA polymerase III (Pol_e), *E. coli* exonuclease domain of Klenow flagment (KF), *C. elegans* CCF-1 (CCF1), and Caf1-like protein of *M. brevicollis* MX1 (MXCaf1). The presumed active site residues are colored in *red*. RNA binding residues in the crystal structure of the hPARN-RNA complex are colored in *green*. The *yellow dots* on the sequences denote the buried residues in the interaction surface with Tob. The secondary structure of hCaf1 is indicated *above* the sequences.

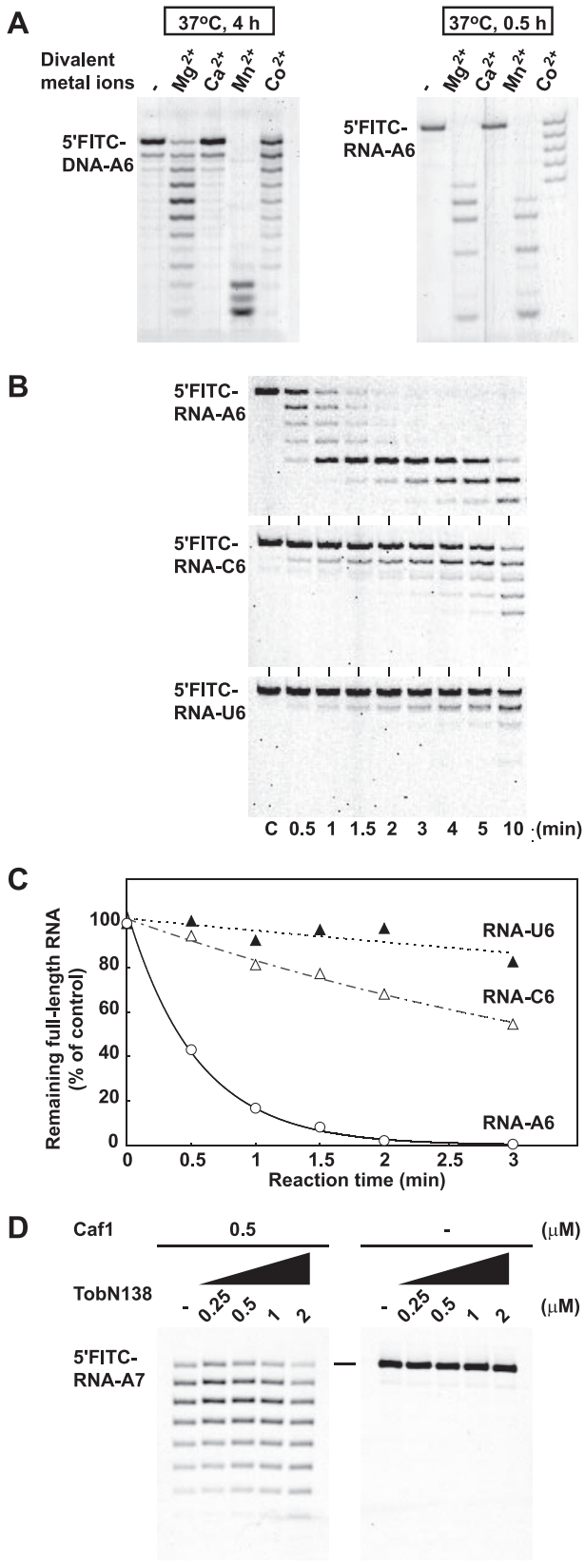

FIGURE 3. **Nuclease activity of hCaf1.** *A*, metal ion-dependent nuclease activity of hCaf1. *Left panel*, hCaf1 was incubated with $MgCl_2$, $CaCl_2$, $MnCl_2$, or $CoCl_2$ at 37 °C for 4 h in the presence of 5′-FITC-labeled DNA-A6. *Right panel*, hCaf1 was incubated with $MgCl_2$, $CaCl_2$, $MnCl_2$, or $CoCl_2$ at 37 °C for 30 min in the presence of 5′-FITC-labeled RNA-A6. *B*, base-specific nuclease activity of hCaf1. hCaf1 was incubated with $MnCl_2$ in the presence of 5′-FITC-labeled RNA-A6, -C6, or -U6 at 37 °C for 0.5, 1, 1.5, 2, 3, 4, 5, or 10 min. As a negative control, a 30-min reaction was carried out in the absence of hCaf1 for each oligonucleotide. *C*, time course of degradation of FITC-labeled RNA by hCaf1. The graph shows the time courses of the degradation of the full-length RNA-A6 (*open circles*), RNA-C6 (*open triangles*), and RNA-U6 (*filled triangles*). The molar ratio of remaining full-length RNA to initial RNA concentration is plotted *versus* the reaction time. The amount of 5′-FITC-labeled full-length RNA was estimated using the software accompanying the FUJI FLA-2000 fluorescent imager. *D*, nuclease activity in the presence of TobN138 of hCaf1. 5′FITC-labeled RNA-A7 in the presence of 0, 0.25, 0.5, 1, and 2 μM TobN138 was incubated with 0.5 μM hCaf1 (*left panel*) and without hCaf1 (*right panel*) at 37 °C for 2 min.

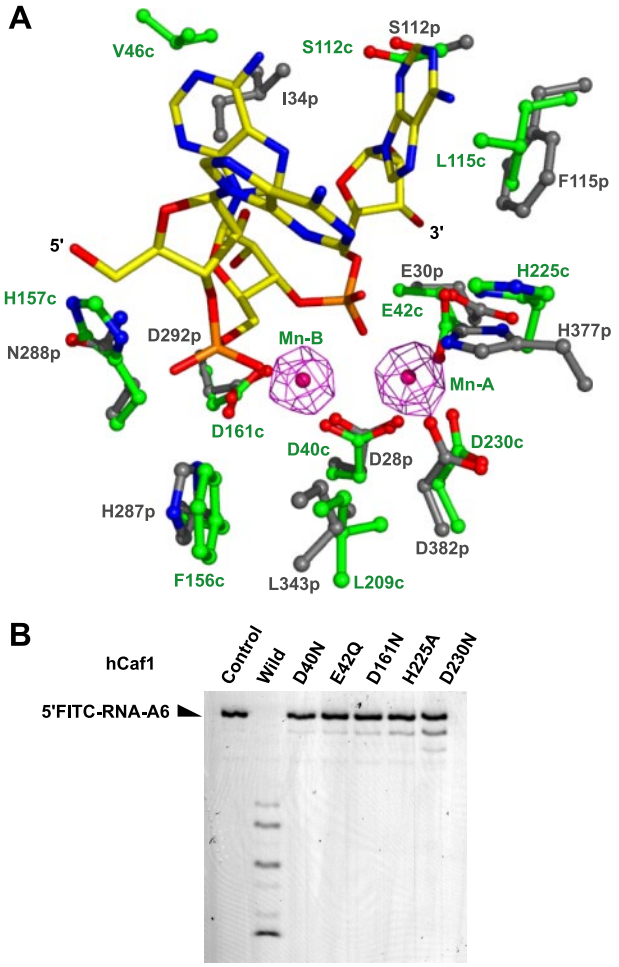

FIGURE 4. **Active site structure and identification of the catalytic residues of hCaf1.** *A*, comparison of the active sites between hCaf1 with Mn^{2+} and hPARN with RNA. The conserved residues critical for nuclease activities are shown. Conserved residues in the catalytic sites of RNase D family proteins are displayed by *ball-and-stick* models colored in *green* and *gray* for hCaf1 and hPARN, respectively. The complex of single-stranded RNA is shown by a *ball-and-stick* model in *yellow*. The electron density map of Mn^{2+} bound to hCaf1 at 6σ is shown as a *pink mesh*. *B*, mutational analysis of the catalytic residues of hCaf1. The presumed active site residues, Asp-40c, Glu-42c, Asp-161c, His-225c, and Asp-230c, were replaced by Asn (D40N), Gln (E42Q), Asn (D161N), Ala (H225A), and Asn (D230N), respectively. Deadenylation by wild type (*Wild*) and each mutant of hCaf1 was examined after 30 min as described in the legend for Fig. 3*B*.

bic pocket in hCaf1. The binding surface is further stabilized by the interactions of Lys-51t in Box A and Glu-105t in Box B with Glu-247c and Tyr-260c, respectively. In addition, an extensive hydrogen bond network mediated by water molecules is formed at the interface.

Conserved residues in Box A and Box B other than those located at the interface are crucial for maintaining the Tob scaf-

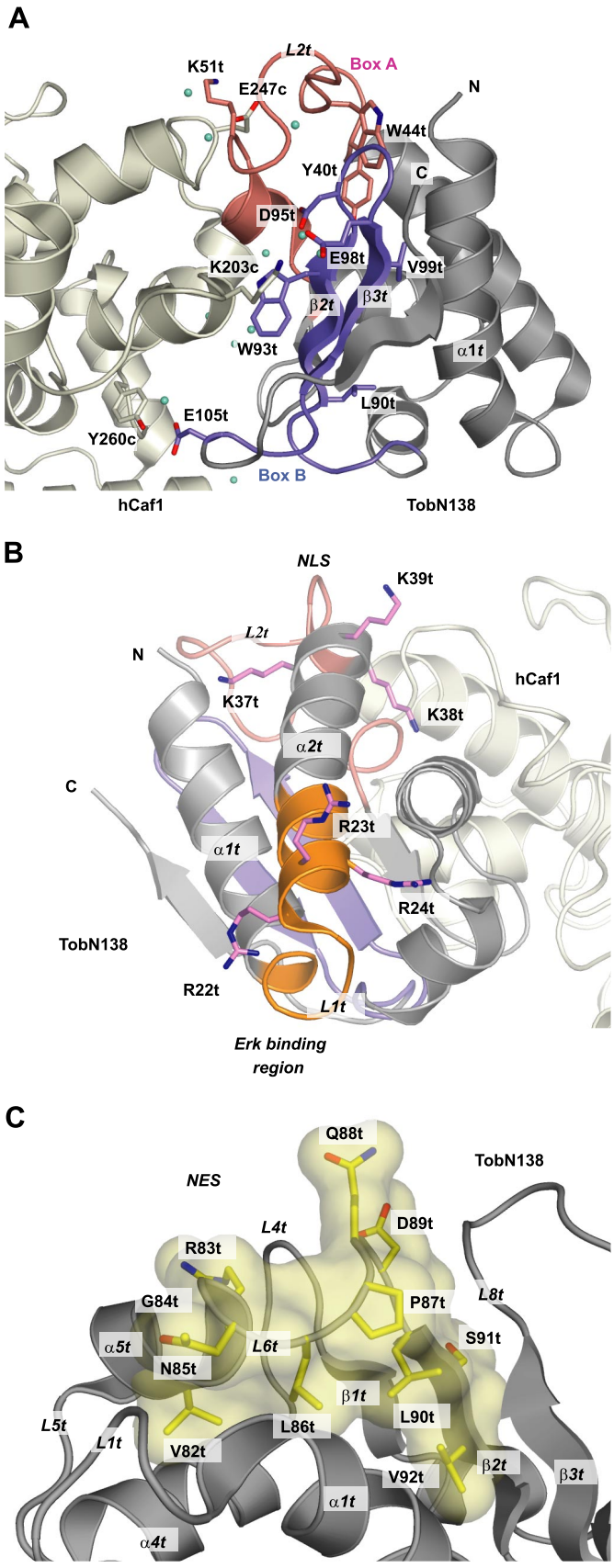

FIGURE 5. **Biologically significant motifs in Tob.** *A*, interaction sites of TobN138 with hCaf1. The residues that mediate the association of TobN138 with hCaf1 are shown as a *stick* model on the ribbon diagram. Water molecules are indicated by *green dots*. Box A and Box B regions of TobN138 are colored *red* and *blue*, respectively. *B*, Erk binding sites on Tob. The Arg residues binding to Erk are indicated as a *stick* model and colored *purple*. The Lys residues identified as the nuclear localization signal are also indicated as a *stick* model and colored *purple*. *C*, putative nuclear export signal (NES82–92) on Tob. The putative nuclear export signal, $LX_{(1-3)}LX_{(2-3)}LXL$, is indicated in *yellow*. The side chains of NES82–92 are shown as a *stick* model.

fold (Figs. 2*A* and 5*A*). For example, the side chain of Tyr-40t forms a hydrophobic core with the side chain of Trp-44t, both of which are located on loop L2t. Also, Leu-90t on strand β2t and Val-99t on strand β3t anchor helix α1t by hydrophobic interactions. The hydrophobic lining is important for the presentation of the conserved residues in Box A and Box B to the interaction with hCaf1.

To confirm whether the interaction surface between TobN138 and hCaf1 observed in the crystal is also maintained in solution, we performed size exclusion chromatography of HisTobN138 in the presence of GST-hCaf1-wild or GST-hCaf1-K203A, which was mutated from Lys-203c to Ala of hCaf1. The size exclusion chromatography that loaded TobN138 and hCaf1-wild exhibited a single peak containing both TobN138 and hCaf1-wild, indicating that TobN138 forms a complex with hCaf1-wild in solution (Fig. 6*A*, *left panel*). On the other hand, the size exclusion chromatography that loaded TobN138 and hCaf1-K203A exhibited two peaks consisting of hCaf1-K203A alone and TobN138 alone, respectively (Fig. 6*A*, *right panel*). Therefore, the interaction surface of the TobN138-hCaf1 complex exhibited in the crystal structure exists in solution.

To confirm whether the interaction surface in the crystal structure is maintained in intact Tob, we next performed a binding assay of intact Tob with hCaf1 using a Strep-Tactin affinity system. Tob was fused to FLAG-tag for immunochemical detection and hCaf1 was fused to Strep-tag II, which binds to Strep-Tactin resin (Fig. 6*B*).

First, Tob and hCaf1 (constructs in Fig. 6*B*) were coexpressed in 293FT cells, and the cell lysate from the transfectants was applied to Strep-Tactin resin. The bound proteins were eluted from the resin by desthiobiotin, and immunochemical detection with anti-FLAG M2 antibody or Strep-tag II antibody confirmed that Tob and TobN138 were bound to hCaf1 *in vivo* (Fig. 6*C*, *lanes 1* and *4*). As expected from the crystal structure of the TobN138-hCaf1 complex, Tob was similarly bound to hCaf1, showing that the BTG/Tob domain of Tob is essential for complex formation. Next, Tob and the hCaf1-K203A mutant, in which Lys-203c was replaced by Ala, were coexpressed and detected by immunoblotting. hCaf1-K203A completely lost the ability to bind to Tob (Fig. 6*C*, *lane 2*), showing that Lys-203c is critical for complex formation in solution as in the crystal structure. Consequently, we confirmed that the interaction surface between TobN138 with hCaf1 in the crystal structure is also conserved even in intact Tob in solution. Finally, Tob and hCaf1-D40N, a mutant deficient in deadenylase activity (Fig. 4*B*), were coexpressed. The complex formation of Tob/hCaf1-D40N was confirmed, indicating that the deadenylase activity of hCaf1 is not related to the complex formation (Fig. 6*C*, *lane 3*).

Erk Binding Site on Tob—Tob is phosphorylated by the mitogen-activated protein kinases Erk1 and Erk2 both *in vivo* and *in vitro* (47, 48). Phosphorylated Tob is translocated from the nucleus to the cytosol, where it is then ubiquiti-

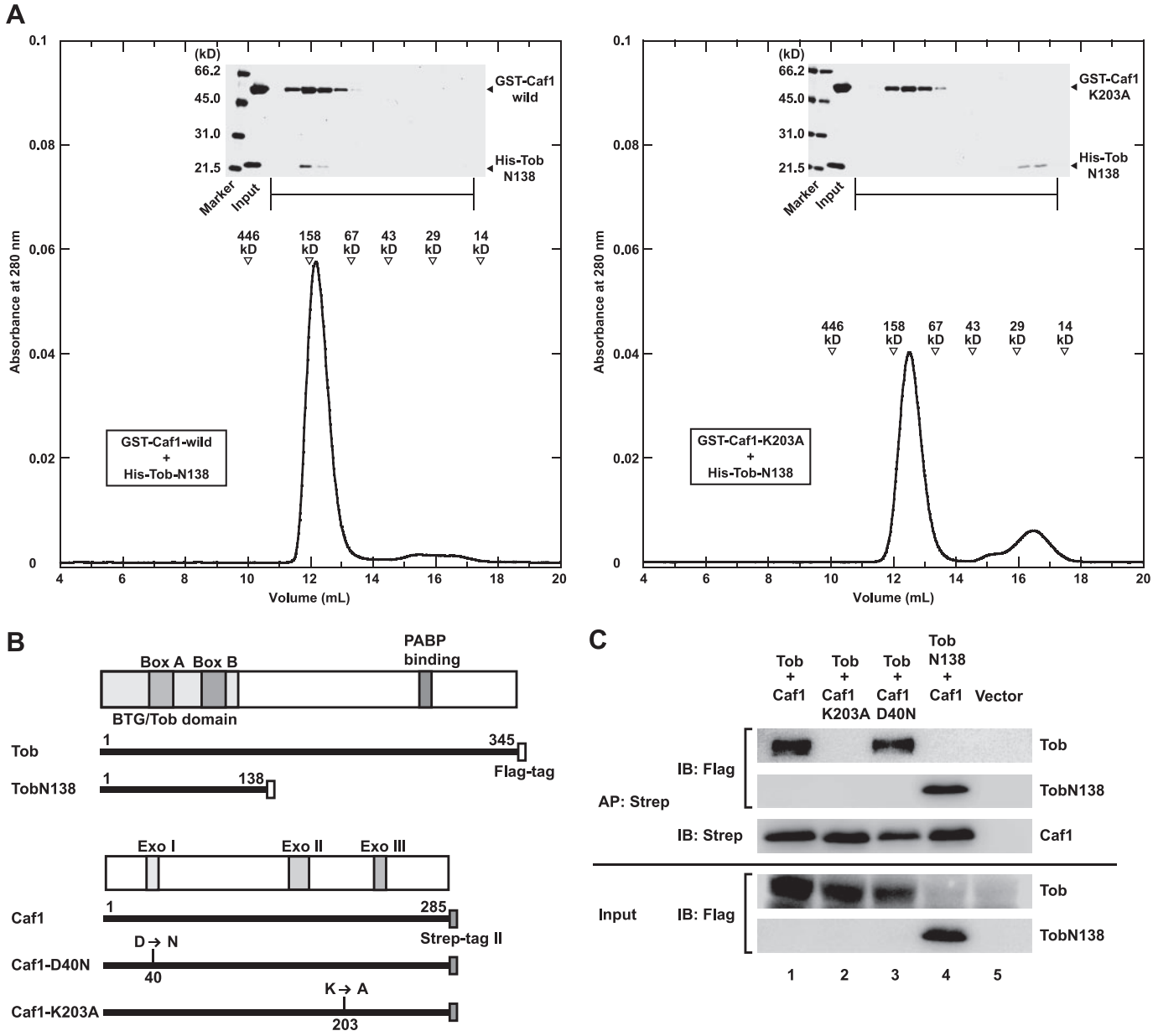

FIGURE 6. **Mutational analysis of the binding site between Tob and hCaf1.** *A*, gel-filtration profiles of the bacterial expressed GST-hCaf1-wild (*left panel*, *bottom*) and GST-hCaf1-k203A (*right panel*, *bottom*) in the presence of HisTobN138 and the Coomassie Blue staining pattern of the corresponding elution fractions (*top* of each *panel*). *B*, schematic representation of the Tob and hCaf1 used for affinity precipitation assays. Tob and TobN138 were fused to FLAG-tag. hCaf1, hCaf1-D40N, and hCaf1-K203A were fused to Strep-tag II. *C*, affinity precipitation assays of FLAG-tagged Tob with Strep-tag II-tagged hCaf1. Tob and hCaf1 were coexpressed in 293FT cells. Cell lysates were subjected to affinity precipitation with Strep-Tactin-Sepharose (*AP: Strep*), and FLAG-tagged or Strep-tag II-tagged proteins were detected by immunoblotting with the anti-FLAG M2 (*IB: Flag*) or anti-Strep-tag II antibody (*IB: Strep*). 2% of cell lysates were used as the Tob and TobN138 input (*Input*).

nated and degraded (49). After degradation, the cell cycle progresses from G_1 to S phase. Erk1/2 has been shown to bind to Arg-22t, Arg-23t, and Arg-24t on Tob (50) (Fig. 2*A*). According to the present crystal structure, these basic residues are located at the N-terminal end of helix α2t (Fig. 5*B*) and are exposed on the opposite side of the hCaf1-binding surface. Therefore, these sites can be accessed easily by Erk1/2 even in the complex. As the nuclear localization signal of Tob includes these Arg residues along with Lys-37t, Lys-38t, and Lys-39t (50) (Figs. 2*A* and 5*B*), the association of Erk1/2 with these basic regions covers the nuclear localization signal and may affect Tob localization.

Nuclear Export Signals of Tob—The subcellular localization of Tob depends on cell cycle progression (36, 50). During progression from G_1 to S phase, Tob is exported from the nucleus to the cytoplasm, a process dependent on the leucine-rich Rev-type nuclear export signal, which has been identified as $LX_{(1-3)}LX_{(2-3)}LXL$ (where *L* is a hydrophobic residue and *X* is any residue) (51, 52). The two nuclear export signals of Tob have been identified at positions 82–92 (NES82–92) (Fig. 2*A*) and 226–234 (NES226–234). In the crystal structure of TobN138, the hydrophobic side chains of NES82–92 are buried to form a hydrophobic interaction with α1t (Fig. 5*C*), and it does not appear to work as an NES.

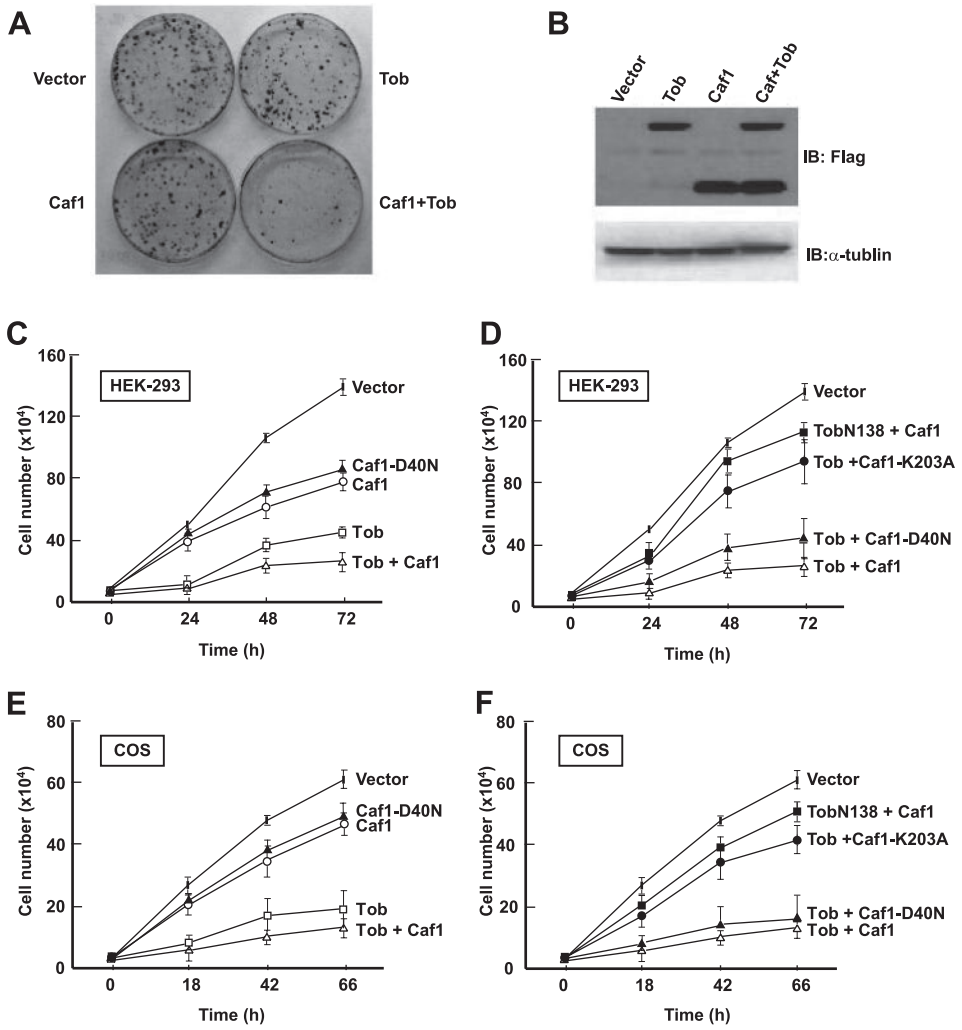

FIGURE 7. **Cell growth experiment using the wild-type and mutants of Tob and hCaf1.** NIH3T3 cells infected with the recombinant retrovirus pME-puro containing FLAG-tagged Tob and/or FLAG-tagged hCaf1. *A*, effect of continuous expression of FLAG-tagged Tob and/or FLAG-tagged hCaf1 on cell growth. Drug-selected cells were seeded at 1×10^3 cells in 60-mm dishes. Ten days after seeding, colonies were stained by the Giemsa staining method. *B*, expression levels of Tob and hCaf1 in the infected cells. The expression of proteins was determined by immunoblotting (*IB*) using an antibody against FLAG-tag. Cell growth assay using HEK-293 (*C* and *D*) and COS-1 (*E* and *F*) cells. HEK-293 and COS-1 cells were seeded at 2×10^4 cells/well, and only gene-expressing cells were selected 18 h after electroporation. *C* and *E*, cell growth curves for Tob, hCaf1, and hCaf1-D40N and the coexpression of Tob with hCaf1. *D* and *F*, cell growth curves for the coexpression of TobN138 with hCaf1, coexpression of Tob with hCaf1-K203A, and coexpression of Tob with hCaf1-D40N. The cell growth curve for the transfection of the vector alone was displayed as a control. Data points represent the mean ± S.E. of triplicate determinations, and the results are representative of 10 experiments ($n = 30$).

Previous studies have shown that NES82–92 does not function as a nuclear export signal, whereas NES226–234 is an efficient NES signal (52), which is consistent with the present crystal structure.

Functional Analysis of the Tob-hCaf1 Complex in Cell Proliferation—To identify the antiproliferative activity of the Tob-hCaf1 complex, we transfected NIH3T3 cells with wild-type Tob, hCaf1, or both using a retrovirus expression system. The single expression of Tob or hCaf1 partially inhibited cell proliferation, whereas cell growth was significantly suppressed in the cells coexpressing both Tob and hCaf1 compared with that of the control cells, although the expression level of each protein was similar (Fig. 7, *A* and *B*). For a more quantitative evaluation of the antiproliferative activity, we tried to analyze the cell lines stably transfected with Tob, hCaf1, or both using a retroviral and various other expression systems. However, we could not achieve the stable coexpression of both Tob and hCaf1 in the cell lines used because of the antiproliferative activities of the Tob/hCaf1 complex.

To evaluate the antiproliferative activity of the Tob-hCaf1 complex more accurately, we measured the growth rates of HEK-293 cells and COS-1 cells that transiently expressed YFP-fused full-length Tob or Tob mutants, CFP-fused hCaf1 or hCaf1 mutants, or both. For adherent cells (COS-1 cells), the cell growth was analyzed in the early phase before the effect of contact inhibition was observed. On the other hand, the analysis of suspension cells (HEK-293 cells) was not affected by the cell density and therefore was free from the effect of contact inhibitions. Transfected cells coexpressing YFP or CFP were selected by flow cytometer and analyzed where the cell numbers for each transfectant were adjusted at the initial stage.

In cells expressing Tob alone, the growth rate was decreased appreciably compared with the control cell growth, and the growth rate of Caf1-expressing cell was twice of that of Tob-expressing cell (Fig. 7, *C* and *E*). However, in the cells coexpressing Tob and hCaf1, the growth rate decreased dramatically (Fig. 7, *C* and *E*). To verify whether growth inhibition depended on the formation of the Tob-hCaf1 complex, we measured the growth rates of the Tob/Caf1-K203A coexpressing cells. The growth rate of the cells coexpressing Tob and hCaf1-K203A was nearly equal to that of the control cells; thus the association between Tob and hCaf1 appears to be crucial for the exertion of a strong antiproliferative activity (Fig. 7, *D* and *F*).

Tob includes a long C-terminal extension outside of the BTG/Tob domain. To confirm whether the BTG/Tob domain exhibits antiproliferative activity, we measured the growth rate of the cells expressing TobN138. Coexpression of TobN138 with hCaf1 had no inhibitory effect on cell growth; thus the BTG/Tob domain alone does not possess any antiproliferative activity (Fig. 7, *D* and *F*). In fact, it is the C-terminal region of Tob that contains the poly(A)-binding protein binding motif and the binding region of the SMAD family protein, which may control translation and transcription (14, 35, 36, 37).

Next, to confirm whether the antiproliferative activity of Tob-hCaf1 depends on the nuclease activity of hCaf1, we measured the growth rate of cells expressing hCaf1-D40N alone, which is deficient in nuclease activity (Fig. 7, *C* and *E*). The growth rate of the hCaf1-D40N-expressing cells was similar to that of wild-type hCaf1. Cells coexpressing Tob with hCaf1-D40N also showed a cell growth rate similar to the cells coexpressing Tob with the wild-type hCaf1, and thus the role of hCaf1 in the antiproliferative activity is not due to its nuclease activity (Fig. 7, *C* and *E*, *D* and *F*). We also obtained similar results using NIH3T3 cells (data not shown).

DISCUSSION

In the present study, we determined the crystal structure of the Tob-hCaf1 complex. Interestingly, both Box A and Box B were aligned on one side of the β-sheet on the BTG/Tob domain. hCaf1 exhibited poly(A)-specific deadenylation activity, which was dramatically increased with manganese ions. Although Tob/BTG domain (TobN138) formed a complex with hCaf1, it did not affect the deadenylation activity. Mutation of Lys-203c, which is the major interaction residue of hCaf1 with Tob in the crystal structure, abolished Tob-hCaf1 complex formation *in vitro* and *in vivo*. To understand the role of Tob and hCaf1 in antiproliferative activity, we measured the growth rate of mammalian cells expressing Tob, hCaf1, and their mutants. The results demonstrated that complex formation between Tob and hCaf1 is crucial for exhibition of antiproliferative activity, whereas nuclease activity of hCaf1 is not required. Furthermore, the C-terminal region of Tob is essential in antiproliferative activity. Thus, intact Tob is indispensable for exertion of antiproliferative activity.

In mammalian cells, poly(A) deadenylation of mRNA is performed by several poly(A)-specific deadenylases, including the CCR4-Not deadenylase complex, Pan2, and PARN. Although the major mammalian deadenylase Pan2 consists of an exonuclease catalytic domain, the degradation activity is insufficient. Pan2 associates with Pan3, which binds with PABPC1, thus tethering mRNA for efficient degradation. Recent reports show that the deadenylase activity of the CCR4-Not complex is enhanced in the presence of Tob and BTG2 (36, 37, 38). Because the C-terminal region of Tob contains a PABP binding motif that associates with PABPC1, it can recruit the poly(A) tail of mRNA to the CCR4-Not complex to facilitate efficient degradation of the poly(A) tail. It is noteworthy that TobN138, which lacks the PABP binding motif, did not exhibit any antiproliferative activity. These data suggest that Tob plays a crucial role in tethering the CCR4-Not complex and PABPC1 and mRNA for efficient degradation of the poly(A) tail.

The CCR4-NOT complex functions as both a transcriptional factor and poly(A)-specific deadenylase (31). Although SMAD family proteins are well known transcriptional factors that bind to the C-terminal region of Tob, there is no evidence to correlate SMAD family proteins to the CCR4-NOT complex. On the other hand, there are several reports that PABP binds to Tob and enhances the deadenylation activity of the CCR4-Not complex (35, 37). These data lead us to the following hypothesis. First, Tob recruits the PABP-mRNA complex to CCR4-NOT complex by binding to Caf1. Therefore, Caf1 serves as a bridge to link Tob and the CCR4-NOT complex rather than as a deadenylase. Next, translation is interrupted by rapid degradation of the poly(A) tail of mRNA. Finally, cell growth is repressed. Further studies are required to elucidate whether the deadenylation level is regulated by formation of the Tob-hCaf1 complex and whether the deadenylation level correlates to antiproliferation activity.

Recently, a similar scenario was reported in that the yeast PUF protein Mpt5p, which binds Pop2, the yeast orthologue of hCaf1 and a component of the CCR4-Not deadenylase complex, stimulated removal of the poly(A) tail of a specfic mRNA. Pop2 was shown to work as a bridge through which the Mpt5p recruited the CCR4-NOT complex to the target mRNA, thereby enhancing deadenylation activity (53).

Interestingly, both the BTG/Tob and Caf1 families are closely related to germ cell differentiation. In Caf1-deficient mice, spermatogenesis is impaired due to incomplete maturation of testicular somatic cells (22, 23). In *C. elegans*, CCF-1 and FOG-3, which are homologues of hCaf1 and Tob, respectively, are essential for germ line development (12, 24). The interaction residues between hCaf1 and Tob in the crystal, such as Lys-203c and Trp-93t, are very similar to Lys-219 of CCF-1 and Phe-91 of FOG-3, respectively. Furthermore, the missense mutations of the BTG/Tob domain of FOG-3 (Fig. 2*A*, *red dot*) probably disrupt the secondary or tertiary structure, which may then fail to associate with CCF1 and may be unable to enter the initial phase of spermatogenesis. FOG-3 may recognize CCF-1 by using Box A and B, which aid germ cell differentiation by controlling mRNA degradation.

In the present study, we showed the importance of specific association of Tob-hCaf1 in antiproliferation. The BTG/Tob family of antiproliferative proteins has been known to associate with the SMAD family (13–16), arginine methyltransferase (17), and histone deacetylase. These binding partners are related to signal transduction, transcription, and duplication. To understand the pleiotropic functions of the BTG/Tob family proteins, further structural and functional studies of the complexes containing BTG/Tob family proteins and their binding partners are required.

Acknowledgments—We thank Dr. Atsushi Nakagawa, Dr. Eiki Yamashita, and all the staff members of the BL44XU Macromolecule Assemblies of Osaka University for assistance with x-ray data collection. We also thank Dr. Koji Nagata for the construction of the pHT1 plasmid.

REFERENCES

1. Tirone, F. (2001) *J. Cell. Physiol.* **187,** 155–165
2. Matsuda, S., Rouault, J., Magaud, J., and Berthet, C. (2001) *FEBS Lett.* **497,** 67–72
3. Matsuda, S., Kawamura-Tsuzuku, J., Ohsugi, M., Yoshida, M., Emi, M., Nakamura, Y., Onda, M., Yoshida, Y., Nishiyama, A., and Yamamoto, T. (1996) *Oncogene* **12,** 705–713
4. Ikematsu, N., Yoshida, Y., Kawamura-Tsuzuku, J., Ohsugi, M., Onda, M., Hirai, M., Fujimoto, J., and Yamamoto, T. (1999) *Oncogene* **18,** 7432–7441
5. Rouault, J. P., Rimokh, R., Tessa, C., Paranhos, G., Ffrench, M., Duret, L., Garoccio, M., Germain, D., Samarut, J., and Magaud, J. P. (1992) *EMBO J.* **11,** 1663–1670
6. Rouault, J. P., Falette, N., Guéhenneux, F., Guillot, C., Rimokh, R., Wang,

Q., Berthet, C., Moyret-Lalle, C., Savatier, P., Pain, B., Shaw, P., Berger, R., Samarut, J., Magaud, J. P., Ozturk, M., Samarut, C., and Puisieux, A. (1996) *Nat. Genet.* **14,** 482–486
7. Fletcher, B. S., Lim, R. W., Varnum, B. C., Kujubu, D. A., Koski, R. A., and Herschman, H. R. (1991) *J. Biol. Chem.* **266,** 14511–14518
8. Bradbury, A., Possenti, R., Shooter, E. M., and Tirone, F. (1991) *Proc. Natl. Acad. Sci. U. S. A.* **88,** 3353–3357
9. Buanne, P., Corrente, G., Micheli, L., Palena, A., Lavia, P., Spadafora, C., Lakshmana, M. K., Rinaldi, A., Banfi, S., Quarto, M., Bulfone, A., and Tirone, F. (2000) *Genomics* **68,** 253–263
10. Yoshida, Y., Matsuda, S., Ikematsu, N., Kawamura-Tsuzuku, J., Inazawa, J., Umemori, H., and Yamamoto, T. (1998) *Oncogene* **16,** 2687–2693
11. Guehenneux, F., Duret, L., Callanan, M. B., Bouhas, R., Hayette, S., Berthet, C., Samarut, C., Rimokh, R., Birot, A. M., Wang, Q., Magaud, J. P., and Rouault, J. P. (1997) *Leukemia* **11,** 370–375
12. Ellis, R. E., and Kimble, J. (1995) *Genetics* **139,** 561–577
13. Yoshida, Y., Nakamura, T., Komoda, M., Satoh, H., Suzuki, T., Tsuzuku, J. K., Miyasaka, T., Yoshida, E. H., Umemori, H., Kunisaki, R. K., Tani, K., Ishii, S., Mori, S., Suganuma, M., Noda, T., and Yamamoto, T. (2003) *Genes Dev.* **17,** 1201–1206
14. Yoshida, Y., Tanaka, S., Umemori, H., Minowa, O., Usui, M., Ikematsu, N., Hosoda, E., Imamura, T., Kuno, J., Yamashita, T., Miyazono, K., Noda, M., Noda, T., and Yamamoto, T. (2000) *Cell* **103,** 1085–1097
15. Yoshida, Y., von Bubnoff, A., Ikematsu, N., Blitz, I. L., Tsuzuku, J. K., Yoshida, E. H., Umemori, H., Miyazono, K., Yamamoto, T., and Cho, K. W. (2003) *Mech. Dev.* **120,** 629–637
16. Tzachanis, D., Freeman, G. J., Hirano, N., van Puijenbroek, A. A., Delfs, M. W., Berezovskaya, A., Nadler, L. M., and Boussiotis, V. A. (2001) *Nat. Immunol.* **2,** 1097–1098
17. Lin, W. J., Gary, J. D., Yang, M. C., Clarke, S., and Herschman, H. R. (1996) *J. Biol. Chem.* **271,** 15034–15044
18. Bogdan, J. A., Bogdan, J. A., Adams-Burton, C., Pedicord, D. L., Sukovich, D. A., Benfield, P. A., Corjay, M. H., Stoltenborg, J. K., and Dicker, I. B. (1998) *Biochem. J.* **336,** 471–481
19. Rouault, J. P., Prévôt, D., Berthet, C., Birot, A. M., Billaud, M., Magaud, J. P., and Corbo, L. (1998) *J. Biol. Chem.* **273,** 22563–22569
20. Prévôt, D., Morel, A. P., Voeltzel, T., Rostan, M. C., Rimokh, R., Magaud, J. P., and Corbo, L. (2001) *J. Biol. Chem.* **276,** 9640–9648
21. Yoshida, Y., Hosoda, E., Nakamura, T., and Yamamoto, T. (2001) *Jpn. J. Cancer Res.* **92,** 592–596
22. Nakamura, T., Yao, R., Ogawa, T., Suzuki, T., Ito, C., Tsunekawa, N., Inoue, K., Ajima, R., Miyasaka, T., Yoshida, Y., Ogura, A., Toshimori, K., Noce, T., Yamamoto, T., and Noda, T. (2004) *Nat. Genet.* **36,** 528–533
23. Berthet, C., Morera, A. M., Asensio, M. J., Chauvin, M. A., Morel, A. P., Dijoud, F., Magaud, J. P., Durand, P., and Rouault, J. P. (2004) *Mol. Cell. Biol.* **24,** 5808–5820
24. Molin, L., and Pusieux, A. (2005) *Gene* **358,** 73–81
25. Draper, M. P., Salvadore, C., and Denis, C. L. (1995) *Mol. Cell. Biol.* **15,** 3487–3495
26. Tuker, M., Valencia-Sanchez, M. A., Staples, R. R., Chen, J., Denis, C. L., and Parker, R. (2001) *Cell* **104,** 377–386
27. Daugeron, M. C., Mauxion, F., and Seraphin, B. (2001) *Nucleic Acids Res.* **29,** 2448–2455
28. Chen, J., Chiang, Y. C., and Denis, C. L. (2002) *EMBO J.* **21,** 1414–1426
29. Tucker, M., Staples, R. R., Valencia-Sanchez, M. A., Muhlrad, D., and Parker, R. (2002) *EMBO J.* **21,** 1427–1436
30. Moser, M. J., Holley, W. R., Chatterjee, A., and Mian, I. S. (1997) *Nucleic Acids Res.* **25,** 5110–5118
31. Denis, C. L., and Chen, J. (2003) *Prog. Nucleic Acid Res. Mol. Biol.* **73,** 221–250
32. Viswanathan, P., Ohn, T., Chiang, Y., Chen, J., and Denis, C. L. (2004) *J. Biol. Chem.* **279,** 23988–23995
33. Bianchin, C., Mauxion, F., Sentis, S., Seraphin, B., and Corbo, L. (2005) *RNA* (*Cold Spring Harbor*) **11,** 487–494
34. Sachs, A. B. (1993) *Cell* **74,** 413–421
35. Okochi, K., Suzuki, T., Inoue, J., Matsuda, S., and Yamamoto, T. (2005) *Genes Cells* **10,** 151–163
36. Ezzeddine, N., Chang, T. C., Zhu, W., Yamashita, A., Chen, C. Y., Zhong, Z., Yamashita, Y., Zheng, D., and Shyu, A. B. (2007) *Mol. Cell. Biol.* **27,** 7791–7801
37. Funakoshi, Y., Doi, Y., Hosoda, N., Uchida, N., Osawa, M., Shimada, I., Tsujimoto, M., Suzuki, T., Katada, T., and Hoshino, S. (2008) *Genes Dev.* **21,** 3135–3148
38. Mauxion, F., Faux, C., and Séraphin, B. (2008) *EMBO J.* **27,** 1039–1048
39. Onishi, M., Kinoshita, S., Morikawa, Y., Shibuya, A., Phillips, J., Lanier, L. L., Gorman, D. M., Nolan, G. P., Miyajima, A., and Kitamura, T. (1996) *Exp. Hematol.* **24,** 324–329
40. Morita, S., Kojima, T., and Kitamura, T. (2000) *Gene Ther.* **7,** 1063–1066
41. Jonstrup, A. T., Andersen, K. R., Van, L. B., and Brodersen, D. E., (2007) *Nucleic Acids Res* **35,** 3153–3164
42. Thore, S., Mauxion, F., Seraphin, B., and Suck, D. (2003) *EMBO Rep.* **4,** 1150–1155
43. Wu, M., Reuter, M., Lilie, H., Liu, Y., Wahle, E., and Song, H. (2005) *EMBO J.* **24,** 4082–4093
44. Hamdan, S., Carr, P. D., Brown, S. E., Ollis, D. L., and Dixon, N. E. (2002) *Structure* (*Lond.*) **10,** 535–546
45. Breyer, W. A., and Matthews, B. W. (2000) *Nat. Struct. Biol.* **7,** 1125–1128
46. Kiefer, J. R., Mao, C., Hansen, C. J., Basehore, S. L., Hogrefe, H. H., Braman, J. C., and Beese, L. S. (1997) *Structure* (*Lond.*) **5,** 95–108
47. Suzuki, T., Kawamura-Tsuzuku, J., Ajima, R., Nakamura, T., Yoshida, Y., and Yamamoto, T. (2002) *Genes Dev.* **16,** 1356–1370
48. Maekawa, M., Nishida, E., and Tanoue, T. (2002) *J. Biol. Chem.* **277,** 37783–37787
49. Sasajima, H., Nakagawa, K., and Yokosawa, H. (2002) *Eur. J. Biochem.* **269,** 3596–3604
50. Kawamura-Tsuzuku, J., Suzuki, T., Yoshida, Y., and Yamamoto, T. (2004) *Oncogene* **23,** 6630–6638
51. Wen, W., Meinkoth, J. L., Tsien, R. Y., and Taylor, S. S. (1995) *Cell* **82,** 463–473
52. Fukuda, M., Gotoh, I., Gotoh, Y., and Nishida, E. (1996) *J. Biol. Chem.* **271,** 20024–20028
53. Goldstrohm, A. C., Seay, D. J., Hook, B. A., and Wickens, M. (2007) *J. Biol. Chem.* **282,** 109–114